genesis 53:573–582 (2015)

RESEARCH ARTICLE

Grhl2 is Required in Nonneural Tissues for Neural Progenitor Survival and Forebrain Development

Chelsea Menke,[1] Megan Cionni,[1] Trevor Siggers,[2,3,4] Martha L. Bulyk,[2,3,5] David R. Beier,[2,3,6] and Rolf W. Stottmann[1,2,3,7]*

[1]Division of Human Genetics, Cincinnati Children's Hospital Medical Center, Cincinnati, Ohio

[2]Division of Genetics, Brigham and Women's Hospital and Harvard Medical School, Boston, Massachusetts

[3]Department of Medicine, Brigham and Women's Hospital and Harvard Medical School, Boston, Massachusetts

[4]Department of Biology, Boston University, Massachusetts

[5]Department of Pathology, Brigham & Women's Hospital and Harvard Medical School, Boston, Massachusetts

[6]Seattle Children's Hospital, Center for Developmental Biology and Regenerative Medicine, Seattle, Washington

[7]Division of Developmental Biology, Cincinnati Children's Hospital Medical Center, Cincinnati, Ohio

Received 18 June 2015; Revised 6 July 2015; Accepted 7 July 2015

Summary: Grainyhead-like genes are part of a highly conserved gene family that play a number of roles in ectoderm development and maintenance in mammals. Here we identify a novel allele of *Grhl2*, *cleft-face 3* (*clft3*), in a mouse line recovered from an ENU mutagenesis screen for organogenesis defects. Homozygous *clft3* mutants have a number of phenotypes in common with other alleles of *Grhl2*. We note a significant effect of genetic background on the *clft3* phenotype. One of these is a reduction in size of the telencephalon where we find abnormal patterns of neural progenitor mitosis and apoptosis in mutant brains. Interestingly, *Grhl2* is not expressed in the developing forebrain, suggesting this is a survival factor for neural progenitors exerting a paracrine effect on the neural tissue from the overlying ectoderm where *Grhl2* is highly expressed. genesis 53:573–582, 2015. © 2015 Wiley Periodicals, Inc.

Key words: ENU; mutagenesis; forebrain; development; mouse; cloning

INTRODUCTION

Embryological development requires the cooperative patterning of cell types from multiple germ layers, which undergo complex morphogenetic movements to create the final body plan. We have been using a forward genetics approach to both identify novel regulators of embryonic organogenesis and to ascertain previously uncharacterized roles for known genes in these processes (Ha *et al*., 2015; Herron *et al*., 2002; Stottmann and Beier, 2010, 2014). This has proven to be an efficient tool for gene and allele discovery. One important outcome from these screens is the recovery of an allelic series of a gene of interest, which may collectively give significant insight into the role of that gene in development that is not evident from a simple null allele.

The *grainyhead* gene was identified in the classic *Drosophila* larval patterning screen (Nusslein-Volhard *et al*., 1984) and has since been implicated in a number of functions such as epidermal barrier maturation, wound repair, tracheal tube size control and CNS development (Almeida and Bray, 2005; Baumgardt *et al*., 2009; Bray and Kafatos, 1991; Cenci and Gould, 2005;

*Correspondence to: Rolf Stottmann, Ph.D. Cincinnati Children's Hospital Medical Center, 3333 Burnet Ave., MLC 7016, Cincinnati, OH 45229, E-mail: rolf.stottmann@cchmc.org

Contract grant sponsor: National Institutes of Health, Contract grant numbers: HD36404, MH081187, HG0003985, and NS085023; Contract grant sponsor: Cincinnati Children's Hospital Research Foundation

Published online 22 July 2015 in
Wiley Online Library (wileyonlinelibrary.com).
DOI: 10.1002/dvg.22875

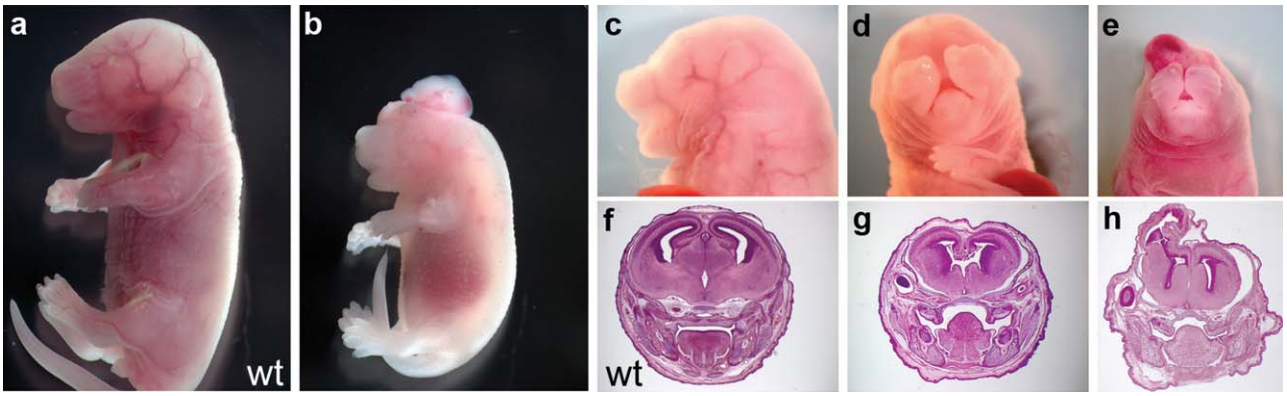

FIG. 1. ***Clft3* phenotypes.** a,b: WT (a) and *clft3* (b) mutant embryo showing the reduced size of the mutant, exencephaly, and edema. c–e: *Cleft face 3* mutants have a variety of anterior phenotypes including shortened snouts (c), failure of anterior midline fusion (d) and growths on top of the head (e). Histological analysis of mutants compared with WT (f) indicates a smaller telencephalon with loss of dorsal midline structures (g) and neuronal overgrowths (h; coronal sections at the approximate level of the eye and teeth). All paired images are shown at the same magnification.

Hemphala *et al*., 2003; Mace *et al*., 2005; Maurange *et al*., 2008; Wang and Samakovlis, 2012). Mammalian genomes have three *Grh* genes (Wilanowski *et al*., 2002), now called *grainyhead-like 1 (Grhl1), Grhl2, Grhl3*. Consistent with the data from Drosophila mutants, the mammalian *grainyhead* gene family has been implicated in developmental process involving the ectoderm. Human mutations have been found in patients with ectodermal dysplasia [*GRHL2*: (Petrof *et al*., 2014)], hearing loss [*GRHL2*; (Peters *et al*., 2002; Van Laer et al., 2008)], and Van der Woude Syndrome [*GRHL3*, (*Peyrard-Janvid et al*., 2014)]. Surprisingly, the development of the CNS has not been studied to date in mammalian *Grh* homologs beyond the role of these genes in neural tube closure.

Here, we describe our identification of an ENU mutation in the mouse in the *Grhl2* gene, which recapitulates many of the previously described phenotypes in other *Grhl2* alleles. Interestingly, our mutation results in a reduction in size of the telencephalon. This phenotype is dependent on the genetic background of the allele and has not previously been reported for mutations in *Grhl2*. We note that expression of *Grhl2* has repeatedly been demonstrated to be confined to the surface ectoderm, suggesting we have identified a novel, nontissue autonomous role for this gene.

RESULTS

Cleft-Face 3 Mutants Have Multiple Defects in Head Development

We originally recovered the *cleft-face3 (clft3)* mutation as part of an ENU mutagenesis screen to identify genes important for development of the mammalian forebrain (Stottmann *et al*., 2011). *Clft3* mutants were initially identified by their significant craniofacial defects at late embryonic stages. Mutants had shorter snouts than wild-type (WT) mice (Fig. 1b,c) and some had a complete failure of tissue fusion in the anterior craniofacial tissues, leading to a cleft face (Fig. 1d,e). Further analysis identified a number of other phenotypes. *Clft3* mutant embryos are often smaller than littermate controls and exhibit edema or appear pale, suggesting a cardiovascular defect (Fig. 1b). We also note incompletely penetrant exencephaly and apparent hemangiomas (Fig. 1b,e) Histological analysis revealed these are, in fact, neuronal overgrowths (Fig. 1h). We also note a hypoplastic telencephalon in *clft3* mutants with defects in dorsal midline structure formation (Fig. 1g).

To study the development of these phenotypes, we performed a phenotypic analysis at multiple stages of embryonic development. The *clft3* phenotype is first evident at E10.5 when a significant proportion of *clft3* mutants are either dead or significantly smaller than littermates (Fig. 2b,d). At E11.5 and E12.5 we began to notice defects in the forebrain, including an obviously smaller telencephalon in relation to the rest of the embryo, in *clft3* mutant embryos (Fig. 2d,f). Even in embryos that are growth retarded, we often note a disproportionate decrease in size of the telencephalon (E11.5). We also noted some embryos with obvious signs of neuronal overgrowths at late organogenesis stages (Fig. 2h).

The *clft3* Mutation Is in the *Grainyhead-like 2* Gene

We took a positional cloning approach to identify the causal mutation in *clft3* mutants. An initial SNP scan of four mutant genomes identified a 72.4 Mb region on chromosome 15 as the only region of shared homozygosity for A/J SNPs among all four embryos tested (proximal end of the chromosome to SNP rs13482643,

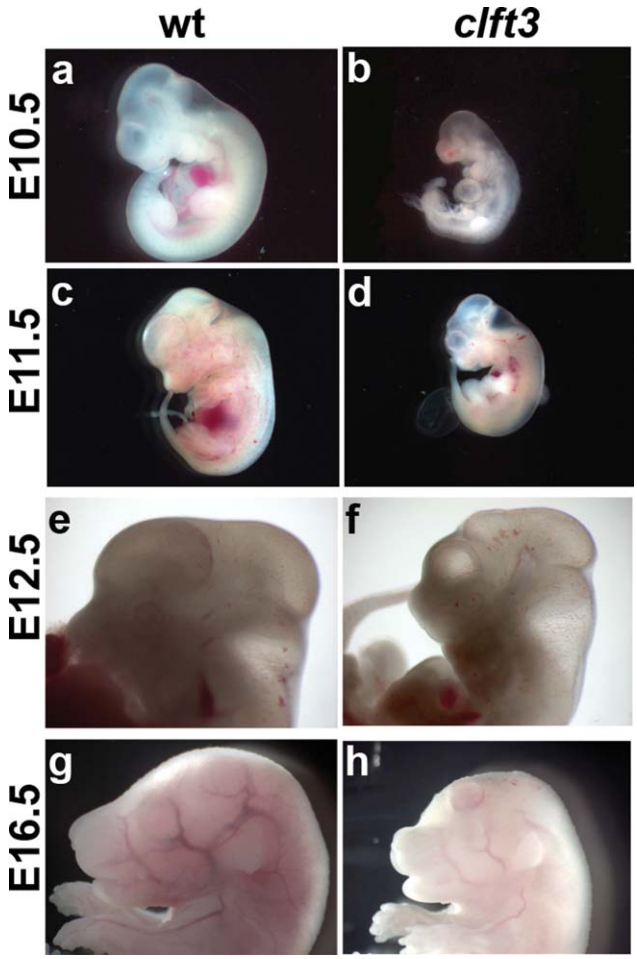

FIG. 2. Developmental analysis of *Clft3* phenotypes. A comparison of WT (a,c,e,g) and *clft3* mutants (b,d,f,h) at E10.5 (a,b), E11.5 (c,d), E12.5 (e,f), and E16.5 (g,h). Mutants are often significantly smaller (b,d) than WT littermates or already dead. Surviving mutants at E11.5 and E12.5 (d,f) show a forebrain which is disproportionately reduced in size. At E16.5 (F), the initial stages of neuronal overgrowth can be seen. All paired images are shown at the same magnification.

Fig. 3a). Further mapping with microsatellite markers and SNPs with multiple affected embryos narrowed the region to a 19.5 Mb interval (D15Mit11 at 31.9Mb to D15Mit228 at 51.4Mb). A literature review on the 60 genes in this minimal interval focusing on gene expression patterns and known loss of function phenotypes suggested *grainyhead-like 2* as a candidate gene for the *clft3* mutation. Sequencing of the *Grhl2* locus from two *clft3* mutants from different litters identified an A-to-G coding change in the eleventh exon of the *Grhl2* locus (c.A1451G; p.D484G, genomic position chr3:37,336,311 GRCm38, mm10; Fig. 3b). The identity of this amino acid sequence in this region of the protein is well conserved among vertebrates and is in the DNA binding domain of this CP2 family transcription factor (Fig. 3c,d). Computational analysis suggests the missense mutation is highly likely to be damaging (Polyphen score of 1.00: "probably damaging: on a scale of 0.00-1.00). Other homologous point mutations from human syndromes cluster in the DNA binding domain as well: Y398H and I428L in ectodermal dysplasia (Petrof *et al.*, 2014).

The *clft3* phenotype has segregated with this mutation for at least twelve generations. Both a custom RFLP and a custom Taqman genotyping assay for the *clft3* mutation have continued to show precise concordance between the *clft3* phenotype (or carrier status in adults) and the c.A1451G variant in the *Grhl2* gene. While there are some subtle differences between the *clft3* allele and previously published alleles of *Grhl2*, the similarity in phenotypes in conjunction with mapping and sequencing data lead us to conclude that *clft3* is most likely a mutation in *Grhl2*.

Clft3 Mutants Show a Background Dependent Phenotype Including Early Embryonic Lethality

The embryonic lethality of homozygous mutants we noted at E10.5 became increasingly penetrant through development (Table 1). In aggregate, mutants are recovered from heterozygous intercrosses at a 19.1% frequency from E9.5-E12.5 and 16.8% frequency from E13.5–E18.5 (both ratios are statistically significantly decreased from the expected 25% as determined by a chi squared analysis). In addition, a significant proportion of the mutants we recovered are either obviously dead or growth retarded and noticeably smaller than their littermates (Table 2). From E10.5 to E12.5, 45.7% of mutants are growth-retarded when compared to littermates and 13.6% are clearly dead or dying. From E12.5 to E18.5, 48.0% of mutants are dead and 12.0% are growth retarded. Heterozygotes survive to weaning in appropriate Mendelian ratios, regardless of genetic background (data not shown).

During the course of our embryonic analysis and outcross breeding to positionally clone the causal mutation in *clft3* mutants, we noted that the phenotype seemed to be getting progressively more severe and the penetrance of some phenotypes was changing. (Note the data presented above and in Tables 1 and 2 are from all experiments combined.) We originally identified *clft3* mutants in the third generation of a recessive screen (Stottmann *et al.*, 2011) in which the G3 mutant embryos would have a significant contribution of the genome from the mutagenized A/J strain (~3/8) and the rest from the FVB/NJ strain (Fig. 4). Details of the mutagenesis strategy can be found elsewhere (Stottmann and Beier, 2010; Stottmann *et al.*, 2011) but, in brief, we mutagenized a population of inbred A/J males (G0, Fig. 4). These were mated with FVB/NJ inbred females to create G1 males, which are genetically 50% from the A/J strain, and 50% FVB/NJ. To homozygose any potential ENU mutations, we again first crossed to

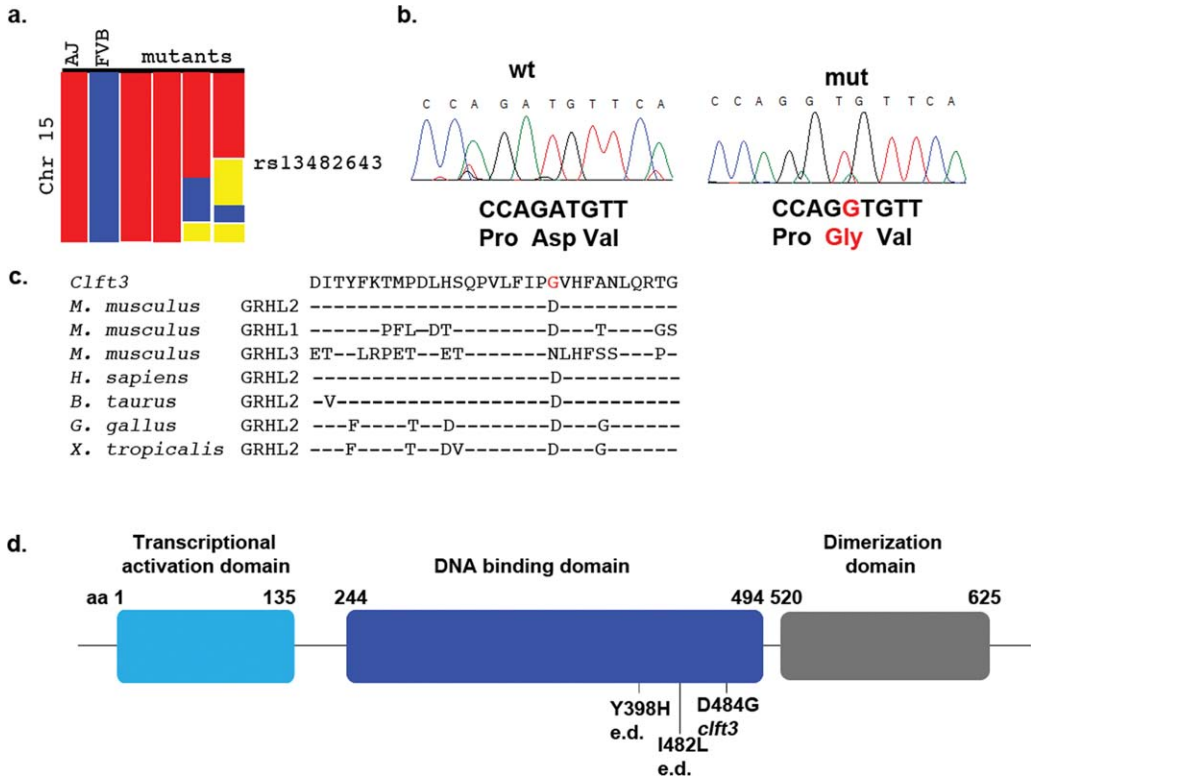

FIG. 3. Cloning of the *clft3* mutation. (a) A whole-genome SNP scan originally identified a region on chromosome 15 containing the *clft3* mutation from the proximal end to SNP rs13482643 (red = homozygous for A/J SNP, blue = homozygous for FVB/NJ SNP, yellow = heterozygous). (b) Sanger sequencing of the *Grhl2* locus identified an A > G missense mutation in *clft3* mutants. (c) The ENU-induced mutation changes the coding of a well-conserved amino acid from aspartic acid to glycine (red text). Amino acid sequence from all three mouse Grhl proteins and Grhl2 sequence from four other vertebrates are indicated (- indicates same residue as above sequence). (D) A graphical representation of the protein domains of Grhl2 shows the *clft3* mutation is in the DNA binding domain (blue) of the Grhl2 protein. The location of point mutations in human ectodermal dysplasia patients (e.d.) are also indicated.

Table 1
A Proportion of Grhl2^{clft3} Homozygous Mutants Do Not Survive To Birth[a]

	Total Mutants		
Age (E)	Embryos	Recovered	Percent
8.5	26	2	7.7
9.5	37	9	24.3
10.5	138	28	20.3
11.5	158	33	20.9
12.5	180	31	17.2*
(E9.5–12.5) 539	*103*	*19.1***	
13.5	71	9	12.7*
14.5	99	16	16.2
16.5	43	12	27.9
17.5	19	3	15.8
18.5	72	11	15.3*
(*E13.5*–E18.5)	304 51	16.8**	
Total	**843**	**154**	**18.3****

[a]Data collected are from all crosses, irrespective of genetic background. Chi-square analyses were performed to indicate mutants are obtained at less than Mendelian ratios (*:$P \leq 0.05$; **:$P \leq 0.01$).

Table 2
A Proportion of Grhl2^{clft3} Homozygous Mutants Are Dead or Growth Retarded

Age (E)	# Mutants	Dead (%)	Small (%)
10.5	22	3 (13.6)	6 (27.2)
11.5	33	5 (15.1)	16 (48.5)
12.5	26	3 (11.5)	15 (57.6)
(E10.5-12.5)	81	11(13.6)	37 (45.7)
13.5	8	2 (25.0)	3 (37.5)
14.5	16	8 (50.0)	1 (6.3)
16.5	12	5 (41.7)	1 (8.3)
17.5	3	3 (100.0)	0
18.5	11	6 (54.5)	1 (9.1)
(E13.5-E18.5)	50	24 (48.0)	6 (12.0)

FVB/NJ females to create the G2 females. These are (as an average) 25% A/J and 75% FVB/NJ, with respect to genetic background. Crossing the G2 females to the G1 males allows recovery of embryos with recessive mutations. These G3 embryos are ~37.5% A/J and 62.5% FVB/NJ. However, as we continue to outcross the carrier animals as part of our cloning strategy, the genetic background will therefore become increasingly the FVBN/J strain (Fig. 4).

In crosses involving the G1 founder, 4/5 mutants had the cleft face phenotype. In the next generation of crosses sired by a G2 male, one 1/195 mutants had a cleft face. Crosses of the G2 male to G2 and G3 females

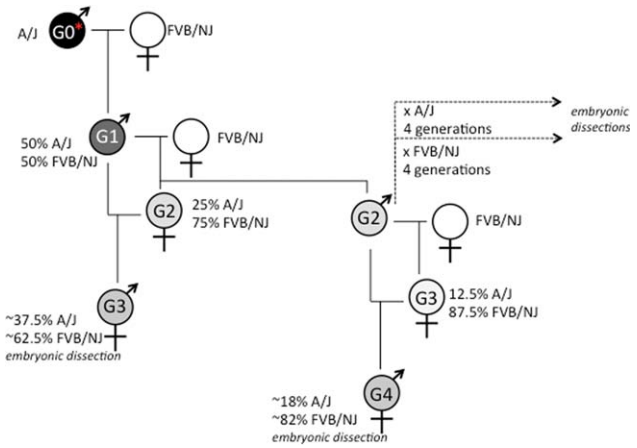

FIG. 4. Breeding strategy for the *clft3* mutation. Details of the breeding are found in the text. The relative shading of gray is to represent the approximate percentage of the genome that comes from the A/J strain (100% = black) as compared to the FVB/NJ strain (100% white). G: generation.

Table 3
Genetic Background Affects Grhl2^{clft3} Phenotype[a]

	FVB/NJ (%)	A/J (%)
Small Body	22 (73.3)	11 (64.7)
Cleft Face	10 (33.3)	6 (35.3)
Exencephaly	1 (3.0)	4 (23.5)
Reduced Telencephalon	11 (36.7)	0
Total Sample	30	17

[a]Phenotypes tallied in a representative sample of embryos from outcrosses of the *clft3* allele.

were combined in this analysis and the single mutant with the cleft face came from a G2 intercross in which the mutant genome would be ~25% derived from the A/J strain, and 75% from the FVB/NJ strain. Subsequently, we created two "substrains" of the *clft3* mutation by outcrossing to A/J and FVBN/J, respectively (Fig. 4). While scoring phenotypes in this analysis, several were found to be significantly affected by genetic background and earlier lethality on the FVBN/J background became evident. We again scored for specific phenotypes after crossing to each strain for at least 4 generations (Table 3). In crosses from FVB/NJ mice at the N4 generation or greater, we note 22/30 (73.3%) have growth retardation, 10/30 (33.3%) have an obviously cleft face, 1/30 (3.0%) had exencephaly and 11/30 (36.7%) have a noticeably smaller telencephalon. In embryos from the A/J "substrain," we note 11/17 (64.7%) have a smaller body, 6/17 (35.3%) have a cleft face, 4/17 (23.5%) have exencephaly and none had the obviously smaller telencephalon. This supported our earlier findings that strain background appears to have an effect on penetrance and expressivity of the *clft3* mutation in mouse. We were unable to maintain the mutation on the A/J background with any efficiency.

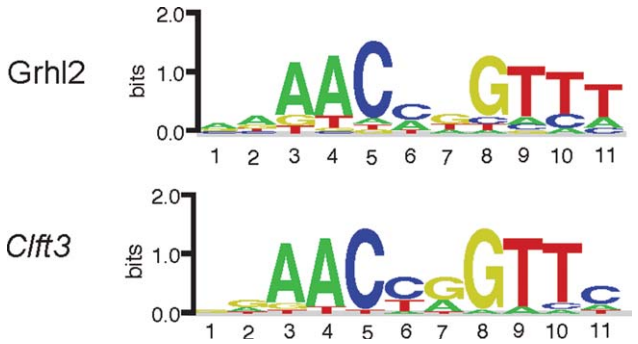

FIG. 5. PBM-determined DNA-binding Motifs for Grhl2 and Clft3. DNA-binding motif logos were determined from the PBM binding data determined for Grhl2 and *Clft3*. Motifs were determined using the Seed-and-Wobble algorithm (see Methods and Materials).

This is likely due to a known reduced fecundity of that strain (Silver, 1995) and/or a maternal effect as has been previously noted (Pyrgaki *et al.*, 2011). Any further embryologic data presented here are from the mouse colony enriched for the FVB background.

WT and clft3 Mutant Grhl2 Proteins Bind DNA with Identical Specificity

The *clft3* mutation is a missense mutation in the DNA binding domain of Grhl2 suggesting it might alter the DNA binding motif for the protein. We tested this hypothesis by performing protein-binding microarray (PBM) experiments for the WT and *clft3* mutant Grhl2 protein (expression of the DNA binding domain as well as flanking sequence). PBM experiments, using the universal PBM design (Berger and Bulyk, 2009; Berger *et al.*, 2006) allow a comprehensive and unbiased assessment of protein-DNA to all possible 8-base pair sequences. PBM experiments performed for the WT and *clft3* mutants showed highly similar DNA binding across the full-range of tested DNA sequences (data not shown), and resulted in identical DNA binding motifs (Fig. 5) that closely resemble the previously reported Grhl2 binding motif (e.g., (Walentin *et al.*, 2015). These results demonstrate that the *clft3* mutant does not change the DNA binding specificity of the mutant protein. However, GRHL2 is known to bind as a dimer and the *clft3* mutation may affect dimer interactions.

Proliferation and Cell Death in the cflt3 Brains

We pursued a molecular analysis to explain the reduction in size of the telencephalon in the *clft3* mutants at E10.5-E12.5 by measuring cell proliferation and cell death with immunohistochemistry for phospho-histone H3 and cleaved caspase 3, respectively. At E10.5, we see no change in the number of pHH3 mitotic cells in the region immediately adjacent to the ventricle ("ventricular") between mutant and WT

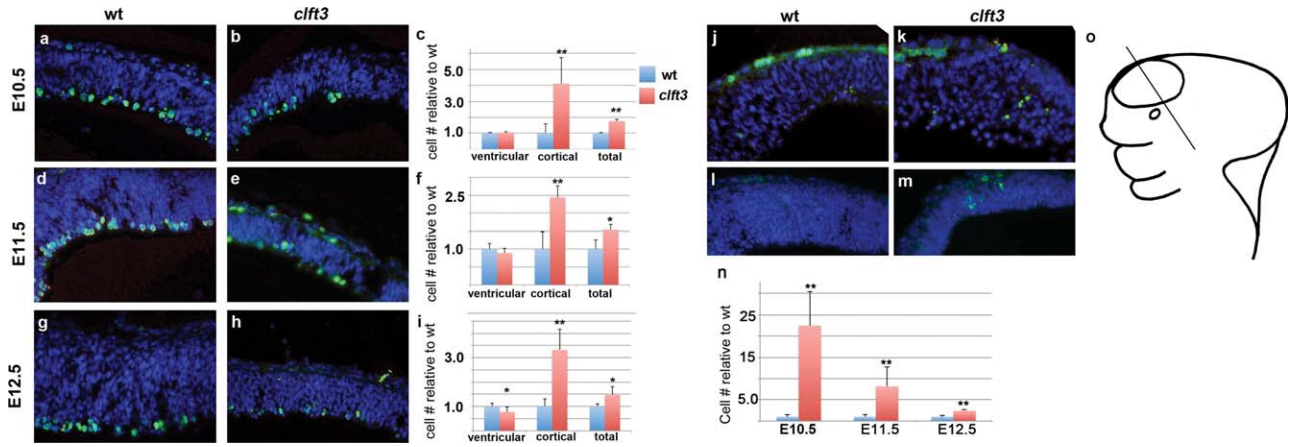

FIG. 6. Molecular analysis of forebrain development in *clft3* mutants. Proliferation analysis with immunohistochemistry for phosphorylated histone H3 (a–i). Representative results are shown for WT (a,d,g) and *clft3* mutants (b,e,h) at E10.5 (a,b), E11.5 (d,e), and E12.5 (g,h). Quantification for each stage is shown in c,f,i. Cells were separately counted in the first cell width immediately adjacent to the ventricle ("ventricular") and the remaining neuroepithelium ("cortical"). Totals of all cells counted are also shown. In each case, the number relative to the WT average is shown. A similar analysis was performed for apoptosis with immunohistochemistry for cleaved-caspase 3 (j–n). Images are shown for E10.5 (j,k) and E11.5 (l,m) from WT (j,k) and *clft3* mutant (K,M). All sections are in the coronal plane from the telencephalic neuroepithelium. Cartoon in (o) shows approximate location of sections in a stylized E11/12 embryo. *: $P \leq 0.05$, **: $P \leq 0.01$.

embryos (Fig. 6a–c). However, we do note a four-fold increase in cells immunoreactive for pHH3, which are not confined to the ventricular region of the neuroepithelium in mutants. These are a small proportion of all dividing cells but the difference in mutants in this subset is striking ("cortical" in Fig. 6c). Combining all mitotic cells we see a 76% increase in pHH3-positive cells in *clft3* mutants at E10.5.

At E11.5, this pattern continues as a true ventricular zone (VZ) emerges and we observe a slight decrease (11%) in VZ pHH3 positive cells in mutants as compared with wt. Again, we see a dramatic increase (244%) in dividing cells in cortical areas outside the VZ. Altogether, these comprise a 53% increase in total cortical mitotic activity (Fig. 6d–f). At E12.5, the VZ mitotic activity is now significantly reduced as compared with WT (Fig. 6g–i). We again see an increase in pHH3-positive cells away from the VZ (333% increase) and, in total, a 47% increase in mitotic activity.

The overall increase in cell proliferation is not consistent with a dramatic reduction in brain size in the *clft3* mutants, so we sought to determine what happened to these cells. We first analyzed levels of programmed cell death with immunohistochemistry for cleaved caspase 3. We see a 22-fold increase at E10.5, an 8-fold increase at E11.5 and a 2.4-fold increase at E12.5. We thus conclude that the *clft3* mutants have the disproportionately small brain largely because of the significantly increased cell death. The proliferation dynamics (increases in numbers of mitotic cells away from the VZ) indicate other dysregulation but these are more than adequately masked by the dramatic increase in cell death suggesting the primary defect leading to the hypoplastic telencephalon is a reduction in cell survival.

DISCUSSION

Here we report a novel ENU-induced allele of *Grhl2*, which results in growth retardation and embryonic lethality with phenotypes in the head including a background dependent reduction in size of the telencephalon. Our data suggest this reduction in size is due to a significant increase in cell death in mutants indicating *Grhl2* is normally acting as an important survival factor during neurogenesis.

The phenotype of *clft3* is consistent with that found for previous genetic ablations of *Grhl2*. The first reported ablation of *Grhl2* was through ES cell mediated homologous recombination [$Grhl2^{tm1.1Jane}$, (Rifat *et al.*, 2010)]. The homozygous null embryos were characterized on a C57BL/6 genetic background and had a fully penetrant anterior craniofacial fusion phenotype. Two independent gene traps were subsequently generated ($Grhl2^{Gt(E115B04)Wrst}$, $Grhl2^{lacz1}$ and $Grhl2^{Gt(RRU622)Byg}$, $Grhl2^{lacZ4}$) and maintained on a mixed 129/B6 background (Werth *et al.*, 2010). These homozygous null mutants were embryonic lethal after E11.5 with anterior spina bifida, exencephaly, split face malformation and growth retardation after the 22 somite stage. Failed closure of the posterior neural tube closure was also noted with lumbosacral spina bifida and curled tail. A third gene trap allele was generated ($Grhl2^{GT(AC0205)Wtsi}$, $Grhl2^{GT}$) which also had an incompletely penetrant cranial neural tube defects (on a B6 genetic background) and lethality prior to E9.5 (Brouns *et al.*, 2011). An independent ENU induced mutation has been identified ($Grhl2^{m1Nisu}$) with similar phenotypes to our *clft3* allele, including very limited survival past E9.5. Finally, a conditional allele has been

generated which also resulted in death by E11.5 when *Grhl2* was deleted throughout the embryo (*Grhl2*^{flox}, (Walentin *et al*., 2015). Given the similarity between our phenotype and those reported for other alleles, and the predicted damaging nature of amino acid substitution, we are confident we have identified the correct mutation.

Differing phenotypes resulting from loss of *Grhl2* on different genetic backgrounds as we report here has been previously noted, although A/J has not been one of the strains reported to date. A/J is not a commonly used strain for maintaining alleles but is able to withstand larger doses of ENU (Justice *et al*., 2000), so is used often in our mutagenesis strategy. Brouns *et al* (Brouns *et al*., 2011) noted that crossing the *Grhl2*^{GT} allele from a mixed 129/B6 background to BALB/c background prolonged the survival of the homozygous mutant embryos past E9.5 and also resulted in a spina bifida phenotype in 88% of mutants. These mice also showed exencephaly and craniofacial defects. Pyrgaki and colleagues (Pyrgaki *et al*., 2011) observed that moving the *Grhl2*^{m1Nisw} allele from the 129 to C3H background allowed some embryos to survive to E18.5; these still had fully penetrant exencephaly and anterior clefting phenotypes. We note that none of the reported alleles have yet been crossed onto either the A/J or FVB/NJ genetic backgrounds that we used in our study. We used these genetic backgrounds because of their utility in ENU mutagenesis and mapping. Some aspects of our phenotype seem to be distinct from alleles reported so far; specifically, the reduction in telencephalon size. We cannot be certain whether this phenotype is then particular to our mutation or the genetic background(s) the alleles are maintained on. However, given the predicted severity of the mutation and the overall similarity between reported phenotypes and ours, we suspect our allele is essentially a null allele, or at least a severe hypomorph, and the differences in phenotypes are indeed due to genetic background effects. It would be intriguing to cross the previously reported alleles onto A/J or FVB/NJ to see if the neural phenotypes we see in our experiments begin to emerge (or to cross *clft3* onto backgrounds similar to the studies described above). Alternatively, a tissue specific ablation could be pursued with the conditional allele (Walentin *et al*., 2015) to circumvent the early lethality and further understand the role of *Grhl2* in survival of the forebrain tissue.

We find the primary molecular explanation for the decreased forebrain is the massive increase in cell death in the homozygous mutants. *Grhl2* has been liked to the control of cell proliferation in a number of different contexts. Morpholino knockdown of *grhl1b* in fish leads to increased apoptosis in the CNS (Dworkin *et al*., 2012). *Grh* also regulates neuroblast proliferation in *Drosophila* (Brody and Odenwald, 2000; Cenci and Gould, 2005; Maurange *et al*., 2008). Interestingly, human ectodermal dysplasia syndrome patients with *GRHL2* mutations had increased Ki67 expression in the skin (Petrof *et al*., 2014). One potential molecular explanation for these changes in proliferation is the finding in multiple systems that *Grhl2* acts within the *Fgf8* signaling pathway. In Drosophila, *branchless*/FGF upregulates *grh* activity post-transcriptionally and this is thought to be due to FGF-induced phosphorylation of grh, most likely by ERK2 (Hemphala *et al*., 2003). *Grh* is also downstream of *erk* signaling in *Drosophila* wound healing. In zebrafish, subphenotypic concentrations of *grhl2b* and *fgf8* morpholino knockdown lead to MHB patterning defects (Dworkin *et al*., 2012). These links to FGF signaling are consistent with the finding FGF is required for neuronal survival in the mouse forebrain (Paek *et al*., 2009).

The most interesting aspect of this forebrain phenotype is that the reduced telencephalic size in *clft3* mutants is apparently regulated by *Grhl2* in a nonautonomous fashion. There is robust data on the expression patterns of *Grhl2* from both of the gene trap alleles as well as the RNA *in situ* hydridization. All current evidence shows *Grhl2* is expressed in the surface ectoderm, including the non-neural ectoderm during early stages of neural tube development (Auden *et al*., 2006; Brouns *et al*., 2011; Pyrgaki *et al*., 2011; Werth *et al*., 2010). None of the available data show any evidence of *Grlh2* expression in the forebrain. Again, the use of the conditional allele of *Grhl2* recently created would be an interesting approach to define the spatiotemporal requirement for *Grhl2* in regulating the survival of the forebrain tissue (Walentin *et al*., 2015).

In conclusion, our findings from the cloning of the *clft3* mouse mutant continue to implicate *Grhl2* in a number of different roles in embryonic development. The nontissue autonomous effect on brain size and the sensitivity of the phenotype to genetic background suggest that *Grhl2* acts within a robust network to guide development of the embryonic ectoderm.

METHODS

Mouse Husbandry

Animals were initially maintained as a mixed A/J, FVB stock. The allele was isolated in an ENU mutagenesis experiment in which A/J males were mutagenized and outcrossed to FVB females (Stottmann *et al*., 2011). Routine genotyping was performed via a RFLP assay wherein the *clft3* mutation creates a *Bstn1* restriction enzyme recognition sequence (F primer: TAAGAT GAGGCCGGTAGCTG; R primer: gagggtgtgagagcaggagt). We also used a custom TaqMan Sample2SNP assay (Assay ID:AHOJB7P, Life Technologies). All animals were maintained in accordance with Brigham and

Women's Hospital and Cincinnati Children's Hospital Medical Center IACUC guidelines. Matings were monitored and noon of the day of copulation plug was determined to be E0.5. Embryos were collected via Cesarean section after the pregnant dams were sedated and euthanized. This line is available to the research community.

Genetic Mapping

The initial mapping of the *clft3* mutant has been described (Stottmann *et al*., 2011). Briefly, an initial genome scan was done with multiple mutant embryos using a 768 marker whole genome SNP panel to identify a region of shared A/J homozygosity among mutants, similar to a method described previously (Moran *et al*., 2006). Microsatellite mapping using standard protocol further localized the mutation as descrived. After identification of the candidate region, exon-directed sequencing revealed the *clft3* mutation in *Grhl2*.

Histology and Immunohistochemistry

Samples for histological analysis were fixed in Bouins fixative, prepared using a Leica TP1020 automated tissue processor, sectioned at 14 μm and stained using established protocols. Paired images presented are of equal magnification. Cryo-sections were used for immunohistochemistry. Antigen retrieval was performed with an Antigen Unmasking Solution (Vector Laboratories) in a microwave. Sections were blocked with 5% Normal Goat Serum/PBST and primary antibodies were incubated overnight. Primary antibodies used in this study were anti-Phospho-Histone H3 (pHH3, SIGMA, 1:500) and cleaved caspase-3 (Cell Signaling, 1:300,). Sections were rinsed with PBST and incubated with an Alexa-Fluor 488 Goat anti-Rabbit secondary antibody (Molecular Probes, 1:500) for one hour at room temperature. Sections were stained with DAPI to visualize cell nuclei and slides were mounted in ProLong AntiFade (Invitrogen) and sealed. Microscopy was performed on a Zeiss AxioImager and cell count analysis was completed using IMARIS 7.5.1 software.

Quantification of Immunohistochemistry

Quantification of mitotic and apoptotic cells was performed by counting fields of cells parallel to the VZ with Imaris 7.5.1. Cells immunoreactive for pHH3 or cleaved caspase 3 were counted as a proportion of all cells in the defined field (DAPI-positive). All statistical analyses were performed in Excel.

Protein Samples and PBM Experiments

Residues 196-625 of *Grhl2* open reading frame (cDNA primers GGGGACAAGTTTGTACAAAAAAG CAGGCTCCTAGCCAGCCACAGCTCCTAT and GGGGAC CACTTTGTACAAGAAAGCTGGGTCTATCAGATCTCCAT CAGCGTGAT) was cloned into the bacterial expression vector pDEST15 to make GST-fusion protein. Site-directed mutagenesis was performed on the *Grhl2* pDEST15 vector to recapitulate the *clft3* mutation. Proteins (WT and mutant) were expressed in *E. coli* BL21 (DE3) cells at 37°C for 2 h, and purified by GST affinity column. PBM experiments were performed using a custom-designed, universal 'all-10mer' microarray (Agilent Technologies Inc., AMADID #016060, 4x44K array format (Zhu *et al*., 2009) described previously (Berger *et al*., 2006). PBM experiments were performed as described previously (Siggers *et al*., 2014).

LITERATURE CITED

Almeida MS, Bray SJ. 2005. Regulation of post-embryonic neuroblasts by Drosophila Grainyhead. Mech Dev 122:1282–1293.

Auden A, Caddy J, Wilanowski T, Ting SB, Cunningham JM, Jane SM. 2006. Spatial and temporal expression of the Grainyhead-like transcription factor family during murine development. Gene Expr Patterns 6: 964–970.

Baumgardt M, Karlsson D, Terriente J, Diaz-Benjumea FJ, Thor S. 2009. Neuronal subtype specification within a lineage by opposing temporal feed-forward loops. Cell 139:969–982.

Berger MF, Bulyk ML. 2009. Universal protein-binding microarrays for the comprehensive characterization of the DNA-binding specificities of transcription factors. Nat Protoc 4:393–411.

Berger MF, Philippakis AA, Qureshi AM, He FS, Estep PW III, Bulyk ML. 2006. Compact, universal DNA microarrays to comprehensively determine transcription-factor binding site specificities. Nat Biotechnol 24:1429–1435.

Bray SJ, Kafatos FC. 1991. Developmental function of Elf-1: an essential transcription factor during embryogenesis in Drosophila. Genes Dev 5:1672–1683.

Brody T, Odenwald WF. 2000. Programmed transformations in neuroblast gene expression during Drosophila CNS lineage development. Dev Biol 226:34–44.

Brouns MR, De Castro SC, Terwindt-Rouwenhorst EA, Massa V, Hekking JW, Hirst CS, Savery D, Munts C, Partridge D, Lamers W, Kohler E, van Straaten HW, Copp AJ, Greene ND. 2011. Over-expression of Grhl2 causes spina bifida in the Axial defects mutant mouse. Hum Mol Genet 20:1536–1546.

Cenci C, Gould AP. 2005. Drosophila Grainyhead specifies late programmes of neural proliferation by regulating the mitotic activity and Hox-dependent apoptosis of neuroblasts. Development 132:3835–3845.

Dworkin S, Darido C, Georgy SR, Wilanowski T, Srivastava S, Ellett F, Pase L, Han Y, Meng A, Heath JK, Lieschke GJ, Jane SM. 2012. Midbrain-hindbrain

boundary patterning and morphogenesis are regulated by diverse grainy head-like 2-dependent pathways. Development 139:525–536.

Ha S, Stottmann RW, Furley AJ, Beier DR. 2015. A forward genetic screen in mice identifies mutants with abnormal cortical patterning. Cereb Cortex 25:167–179.

Hemphala J, Uv A, Cantera R, Bray S, Samakovlis C. 2003. Grainy head controls apical membrane growth and tube elongation in response to Branchless/FGF signalling. Development 130:249–258.

Herron BJ, Lu W, Rao C, Liu S, Peters H, Bronson RT, Justice MJ, McDonald JD, Beier DR. 2002. Efficient generation and mapping of recessive developmental mutations using ENU mutagenesis. Nat Genet 30: 185–189.

Justice MJ, Carpenter DA, Favor J, Neuhauser-Klaus A, Hrabe de Angelis M, Soewarto D, Moser A, Cordes S, Miller D, Chapman V, Weber JS, Rinchik EM, Hunsicker PR, Russell WL, Bode VC. 2000. Effects of ENU dosage on mouse strains. Mamm Genome 11:484–488.

Mace KA, Pearson JC, McGinnis W. 2005. An epidermal barrier wound repair pathway in Drosophila is mediated by grainy head. Science 308:381–385.

Maurange C, Cheng L, Gould AP. 2008. Temporal transcription factors and their targets schedule the end of neural proliferation in Drosophila. Cell 133:891–902.

Moran JL, Bolton AD, Tran PV, Brown A, Dwyer ND, Manning DK, Bjork BC, Li C, Montgomery K, Siepka SM, Vitaterna MH, Takahashi JS, Wiltshire T, Kwiatkowski DJ, Kucherlapati R, Beier DR. 2006. Utilization of a whole genome SNP panel for efficient genetic mapping in the mouse. Genome Res 16:436–440.

Nusslein-Volhard C, Wieschaus E, Kluding H. 1984. Mutations affecting the pattern of the larval cuticle in *Drosophila melanogaster*. I. Zygotic loci on the second chromosome. Wilhelm Roux's Arch Dev Biol 193:267–282.

Paek H, Gutin G, Hebert JM. 2009. FGF signaling is strictly required to maintain early telencephalic precursor cell survival. Development 136:2457–2465.

Peters LM, Anderson DW, Griffith AJ, Grundfast KM, San Agustin TB, Madeo AC, Friedman TB, Morell RJ. 2002. Mutation of a transcription factor, TFCP2L3, causes progressive autosomal dominant hearing loss, DFNA28. Hum Mol Genet 11:2877–2885.

Petrof G, Nanda A, Howden J, Takeichi T, McMillan JR, Aristodemou S, Ozoemena L, Liu L, South AP, Pourreyron C, Dafou D, Proudfoot LE, Al-Ajmi H, Akiyama M, McLean WH, Simpson MA, Parsons M, McGrath JA. 2014. Mutations in GRHL2 result in an autosomal-recessive ectodermal Dysplasia syndrome. Am J Hum Genet 95:308–314.

Peyrard-Janvid M, Leslie EJ, Kousa YA, Smith TL, Dunnwald M, Magnusson M, Lentz BA, Unneberg P, Fransson I, Koillinen HK, Rautio J, Pegelow M, Karsten A, Basel-Vanagaite L, Gordon W, Andersen B, Svensson T, Murray JC, Cornell RA, Kere J, Schutte BC. 2014. Dominant mutations in GRHL3 cause Van der Woude Syndrome and disrupt oral periderm development. Am J Hum Genet 94:23–32.

Pyrgaki C, Liu A, Niswander L. 2011. Grainyhead-like 2 regulates neural tube closure and adhesion molecule expression during neural fold fusion. Dev Biol 353:38–49.

Rifat Y, Parekh V, Wilanowski T, Hislop NR, Auden A, Ting SB, Cunningham JM, Jane SM. 2010. Regional neural tube closure defined by the Grainy head-like transcription factors. Dev Biol 345:237–245.

Siggers T, Reddy J, Barron B, Bulyk ML. 2014. Diversification of transcription factor paralogs via noncanonical modularity in C2H2 zinc finger DNA binding. Mol Cell 55:640–648.

Silver LM. 1995. Mouse genetics: Concepts and applications. New York: Oxford University Press. p xiii, 362 p.

Stottmann R, Beier D. 2014. ENU Mutagenesis in the Mouse. Curr Protoc Hum Genet 82:151411–151410.

Stottmann RW, Beier DR. 2010. Using ENU mutagenesis for phenotype-driven analysis of the mouse. Methods Enzymol 477:329–348.

Stottmann RW, Moran JL, Turbe-Doan A, Driver E, Kelley M, Beier DR. 2011. Focusing forward genetics: A tripartite ENU screen for neurodevelopmental mutations in the mouse. Genetics 188:615–624.

Van Laer L, Van Eyken E, Fransen E, Huyghe JR, Topsakal V, Hendrickx JJ, Hannula S, Maki-Torkko E, Jensen M, Demeester K, Baur M, Bonaconsa A, Mazzoli M, Espeso A, Verbruggen K, Huyghe J, Huygen P, Kunst S, Manninen M, Konings A, Diaz-Lacava AN, Steffens M, Wienker TF, Pyykko I, Cremers CW, Kremer H, Dhooge I, Stephens D, Orzan E, Pfister M, Bille M, Parving A, Sorri M, Van de Heyning PH, Van Camp G. 2008. The grainyhead like 2 gene (GRHL2), alias TFCP2L3, is associated with age-related hearing impairment. Hum Mol Genet 17:159–169.

Walentin K, Hinze C, Werth M, Haase N, Varma S, Morell R, Aue A, Potschke E, Warburton D, Qiu A, Barasch J, Purfurst B, Dieterich C, Popova E, Bader M, Dechend R, Staff AC, Yurtdas ZY, Kilic E, Schmidt-Ott KM. 2015. A Grhl2-dependent gene network controls trophoblast branching morphogenesis. Development 142:1125–1136.

Wang S, Samakovlis C. 2012. Grainy head and its target genes in epithelial morphogenesis and wound healing. Curr Top Dev Biol 98:35–63.

Werth M, Walentin K, Aue A, Schonheit J, Wuebken A, Pode-Shakked N, Vilianovitch L, Erdmann B, Dekel B, Bader M, Barasch J, Rosenbauer F, Luft FC, Schmidt-Ott KM. 2010. The transcription factor grainyhead-like 2 regulates the molecular composition of the epithelial apical junctional complex. Development 137:3835–3845.

Wilanowski T, Tuckfield A, Cerruti L, O'Connell S, Saint R, Parekh V, Tao J, Cunningham JM, Jane SM. 2002. A highly conserved novel family of mammalian developmental transcription factors related to Drosophila grainyhead. Mech Dev 114:37–50.

Zhu C, Byers KJ, McCord RP, Shi Z, Berger MF, Newburger DE, Saulrieta K, Smith Z, Shah MV, Radhakrishnan M, Philippakis AA, Hu Y, De Masi F, Pacek M, Rolfs A, Murthy T, Labaer J, Bulyk ML. 2009. High-resolution DNA-binding specificity analysis of yeast transcription factors. Genome Res 19:556–566.